

# Nonlocal density-wave theory for gravitational instability of protoplanetary disks

G. Rüdiger<sup>1</sup> and L. L. Kitchatinov<sup>1,2</sup>

<sup>1</sup> Astrophysikalisches Institut Potsdam, An der Sternwarte 16, D-14482 Potsdam, Germany (gruediger@aip.de, lkitchatinov@aip.de)

<sup>2</sup> Institute for Solar-Terrestrial Physics, P.O. Box 4026, Irkutsk, 664033, Russia (kit@iszf.irk.ru)

December 10, 1997

**Abstract.** Stability of self-gravitating infinitesimally thin gaseous disks rotating around a central mass is studied. Our linear but global analysis concerns marginal stability, i.e. it yields the critical temperature for onset of the instability for any given ratio of the disk mass to the central mass. Axisymmetric and low- $m$  nonaxisymmetric excitations are analyzed. The axial symmetry preferred by the instability changes from rings ( $m = 0$ ) to one-armed trailing spirals ( $m = 1$ ) with increase of the fractional disk mass. Distribution of the surface density along the spiral arms is not uniform but describes a sequence of maxima which may be identified with forming planets. The number of the mass concentrations decrease with increasing fractional disk mass.

The solutions in the form of global nonaxisymmetric vortices are also obtained. The vortices are never found to be unstable, however.

**Key words:** accretion disks – instabilities – planetary systems

## 1. Introduction

The recent detections of exosolar planets like that around 51 Peg yield the data for studies of the general structure of extra-solar planetary systems. Number, size and the orbit geometry of the planets in various types of planetary systems may now be expected to form the database for testing the theoretical concepts. The first question is, of course, whether our solar system forms a rule or an exception in nature.

It is not very new to consider the solar system as the relict of a global instability in the context of the density-wave theory. Such a concept, certainly, has its roots in

the fascinating order in the observed planetary orbits suggesting a global formation process rather than a local, i.e. a small-scaled one. The density-wave theory in its short-wave approximation is here faced with difficulties. Both mass and temperature of the protoplanetary disk prove to be rather restricted if the theory is applied to the original thin Keplerian disk. Those modes with a wave number

$$k_{\text{crit}} = \frac{1}{\pi} \frac{M_*}{\Sigma_0 r^3} \quad (1)$$

become unstable if the Toomre parameter,

$$Q = \frac{\Omega c_{\text{ac}}}{\pi G \Sigma_0}, \quad (2)$$

sinks below unity (Toomre 1964; Safronov 1969; Goldreich & Ward 1973). With the standard notations,  $G$  is the gravity constant,  $M_*$  is the central mass,  $c_{\text{ac}}$  is the speed of sound,  $\Omega$  is the angular velocity and  $\Sigma_0$  is the surface density of the disk. Equation (1) can be easily rewritten as

$$M_{\text{disk}} \simeq M_* / kr, \quad (3)$$

so that the observed

$$\Delta r / r \simeq 0.5 \quad (4)$$

(Nieto 1972; Lissauer & Cuzzi 1985), i.e.  $kr \approx 10$ , forces the disk to be rather massive in contrast to the normally assumed low mass ( $M_{\text{disk}} \ll M$ ). Moreover, too massive disks do not obey the Keplerian rotation law. There are thus difficulties with application of (1) to the observed scales and masses (Polyachenko & Fridman 1972; Cameron 1978).

On the other hand, with the sound speed  $c_{\text{ac}} = \sqrt{\mathcal{R}T}$  the instability condition reads

$$T \lesssim \frac{\pi^2 \Sigma_0^2 G r^3}{\mathcal{R} M_\odot} \approx 10^{-2} \Sigma_3^2 r_{\text{AU}}^3 \quad (5)$$

with  $\Sigma_3 = \Sigma_0/(10^3 \text{ g cm}^{-2})$  and  $r_{\text{AU}} = r/1\text{AU}$ . In the Earth region ( $\Sigma_3 \approx 1$ ) the disk must thus be much cooler than it is reasonable to assume (Goldreich & Ward 1973). As numerical simulations with a big number of mass points (Cassen et al. 1981) generally confirm the stability criterion,  $Q > 1$ , there is little hope for a gaseous disk to be sufficiently cold.

With most optimistic estimations, a very thin dust layer which forms slowly in the disk's mid-plane could be cold enough. It may have a very low temperature according to  $c_{\text{ac}} \simeq H\Omega$  with  $H$  of the order 'meter' (Nakagawa et al. 1981). Once the dust disk is sufficiently thin, the parameter  $Q$  becomes subcritical and the disk begins to fragment into a number of rings. Their distances, however, are too small as the surface density of the dust disk is low. With the often quoted value of  $100 \text{ g cm}^{-2}$ , Weidenschilling (1977) obtained  $kr \sim 10^4$ . The resulting mass concentrations exhibit maximally  $10^{18} \text{ g}$  in the Earth region and must be defined as 'planetesimals' (Safronov 1969; Safronov & Ruzmaikina 1985; Hayashi et al. 1985). The large value of  $kr$  also ensures here the applicability of the short-wave approximation on which all the above considerations are based.

In the context of the density-wave theory for planetary systems the question of whether the aforementioned problems survive within a *nonlocal* formalism remains open. A single wave number has a restricted meaning with such a formulation. Only a spectrum serves as a characteristics of the resulting global pattern. The critical temperature below which a global structure is excited is the main output of such a formulation.

With the global approach significant progress has been made in explaining the spiral structure of galaxies within the density-wave theory. Besides a detailed discussion of the dispersion relation for tightly wound spirals, the instability of global modes has been analyzed with considerable success (Lin & Shu 1964; Aoki & Iye 1978; Aoki et al. 1979; Haass 1983; Meinel 1983; see also Binney & Tremaine 1987).

For protoplanetary disks Rüdiger & Tschäpe (1987) tried to break the short-wave approximation by employing a relation between potential disturbances and density disturbances given by Bertin and Mark (1979). In contrast to the earlier treatments (cf. Shu 1985), it incorporates terms up to the second order in  $kr$ . Rüdiger & Tschäpe (1987) studied numerically the resulting dispersion relation and found indication for existence of an instability of non-short ring-like disturbances. It could be more plausible to realize the Titus-Bode law as the maxima series of density rings with low disk mass than in the afore-going discussion. One of the two basic difficulties of the density-wave theory for the protoplanetary disks seems to be weakened along this way. As, however, the implication of non-short waves leads into the domain of global modes one has to develop a truly non-local formulation for consistency.

Another aim of the present work is to find whether axisymmetric or nonaxisymmetric modes are more unstable. Are rings or spirals excited once the cooling of a protoplanetary disk brings it to an unstable state? From this point of view we may see close relations to the phenomena of symmetry breaking by hydrodynamic and magnetohydrodynamic instabilities, to the planetary and stellar mean-field dynamo theory, to the rotating protostars (Yang et al. 1991) and spiral wave excitation in galaxies (Hohl 1971; Bertin 1983; Monaghan & Lattanzio 1991). Also the stability or fragmentation problem for uniformly rotating self-gravitating stellar or gaseous disks (Vauterin & Dejonghe 1995; Köhler 1995; Fuchs 1996) generally belongs to the theory presented in the present paper.

Further, we mention the suggestion by Morfill et al. (1993) that the existence of ring-like structures may help to overcome one of the main difficulties of the standard accretion disk theory, i.e. the disagreement between the theoretically predicted and observed radial temperature profiles (Beckwith 1994).

## 2. The basic equations

Small disturbances in an infinitesimally thin inviscid disk in a generally nonuniform rotation are considered. We assume the linear relation between the pressure and density excitations,

$$p' = c_{\text{ac}}^2 \rho', \quad (6)$$

valid for isothermal as well as for isentropic discs. Then the linearized equations for the radial ( $u'$ ) and azimuthal ( $v'$ ) velocity disturbances and the continuity equation read

$$\begin{aligned} \frac{\partial u'}{\partial t} + \Omega \frac{\partial u'}{\partial \phi} - 2\Omega v' + \frac{\partial \psi'}{\partial r} + \frac{\partial}{\partial r} \frac{c_{\text{ac}}^2 \Sigma'}{\Sigma_0} &= 0, \\ \frac{\partial v'}{\partial t} + \Omega \frac{\partial v'}{\partial \phi} + \frac{\kappa^2}{2\Omega} u' + \frac{1}{r} \frac{\partial \psi'}{\partial \phi} + \frac{c_{\text{ac}}^2}{\Sigma_0 r} \frac{\partial \Sigma'}{\partial \phi} &= 0, \\ \frac{\partial \Sigma'}{\partial t} + \Omega \frac{\partial \Sigma'}{\partial \phi} + \frac{1}{r} \frac{\partial (u' r \Sigma_0)}{\partial r} + \frac{\Sigma_0}{r} \frac{\partial v'}{\partial \phi} &= 0, \end{aligned} \quad (7)$$

with  $\kappa$  being the epicyclic frequency,

$$\kappa^2 = \frac{2\Omega}{r} \frac{d(r^2\Omega)}{dr}. \quad (8)$$

$\Sigma$  denotes the surface density with  $\Sigma_0$  and  $\Sigma'$  being its equilibrium value and disturbance, respectively, and  $\psi$  is the gravity potential. The potential and density are related by the Poisson equation,

$$\Delta \psi = 4\pi G \Sigma \delta(z) \quad (9)$$

(cf. Möhlmann 1985; Schmit & Tscharnuter 1995). As usual for linear theories, the modes with different azimuthal wave numbers,  $m$ , i.e. those proportional to  $e^{im\phi}$ ,

can be considered independently. Then the Toomre (1964) solution for the Poisson equation applies,

$$\psi' = -2\pi G \int_0^\infty S(k) J_m(kr) e^{im\phi - |kz|} dk, \quad (10)$$

where  $S(k)$  is the density spectrum after the Fourier-Bessel transform

$$\Sigma' = \int_0^\infty J_m(kr) k S(k) dk e^{im\phi}. \quad (11)$$

The existence of general solution (10) of the Poisson equation (9) demonstrates the convenience of the Fourier-Bessel transform. However, the velocity components,  $u'$  and  $v'$ , do not match transformations like (11). It is appropriate to describe the flow in terms of scalar potentials for the momentum density disturbances, i.e.

$$\Sigma_0 u' = \frac{\partial \Phi}{\partial r} + \frac{1}{r} \frac{\partial V}{\partial \phi}, \quad \Sigma_0 v' = \frac{1}{r} \frac{\partial \Phi}{\partial \phi} - \frac{\partial V}{\partial r}. \quad (12)$$

The potentials  $V$  and  $\Phi$  define the vorticity and divergence of the flow, respectively,

$$\text{div}(\Sigma_0 \mathbf{v}') = \Delta_2 \Phi, \quad \text{rot}_z(\Sigma_0 \mathbf{v}') = -\Delta_2 V, \quad (13)$$

where  $\mathbf{v}'$  is the 2D velocity vector and

$$\Delta_2 = \frac{1}{r} \frac{\partial}{\partial r} r \frac{\partial}{\partial r} + \frac{1}{r^2} \frac{\partial^2}{\partial \phi^2} \quad (14)$$

is the 2D Laplacian.

On using Eqs. (12) to (14), the equation system (7) can be reformulated in terms of the flow potentials. Then it reads

$$\begin{aligned} \frac{\partial (\Delta_2 \Phi)}{\partial t} + \Omega \frac{\partial (\Delta_2 \Phi)}{\partial \phi} + \left( \frac{\kappa^2}{\Omega} - 2\Omega \right) (\Delta_2 V) \\ - \left( \frac{\kappa^2}{\Omega} - 4\Omega \right) \frac{\partial}{\partial r} \left( \frac{\partial V}{\partial r} - \frac{1}{r} \frac{\partial \Phi}{\partial \phi} \right) \\ + \frac{d\Sigma_0}{dr} \frac{\partial \psi'}{\partial r} + \Sigma_0 (\Delta_2 \psi') \\ + \Delta_2 (c_{\text{ac}}^2 \Sigma') + \frac{1}{r} \frac{\partial}{\partial r} (n c_{\text{ac}}^2 \Sigma') = 0, \end{aligned}$$

$$\begin{aligned} \frac{\partial (\Delta_2 V)}{\partial t} + \Omega \frac{\partial (\Delta_2 V)}{\partial \phi} - \frac{\kappa^2}{2\Omega} (\Delta_2 \Phi) \\ - \left( \frac{d}{dr} \frac{\kappa^2}{2\Omega} \right) \left( \frac{\partial \Phi}{\partial r} + \frac{1}{r} \frac{\partial V}{\partial \phi} \right) \\ - \frac{1}{r} \frac{d\Sigma_0}{dr} \frac{\partial \psi'}{\partial \phi} + \frac{n c_{\text{ac}}^2}{r^2} \frac{\partial \Sigma'}{\partial \phi} = 0, \end{aligned}$$

$$\frac{\partial \Sigma'}{\partial t} + \Omega \frac{\partial \Sigma'}{\partial \phi} + \Delta_2 \Phi = 0, \quad (15)$$

where

$$n(x) = -\frac{r}{\Sigma_0} \frac{d\Sigma_0}{dr} \quad (16)$$

is the radial slope of the surface density profile.

The linear stability problem can be reduced to the eigenvalue problem by assuming an exponential time dependence. Also the azimuthal wave number can be involved explicitly, so that all the excitations become proportional to  $\exp(\sigma t + im\phi)$ . Next, the equation system is scaled to dimensionless units to read

$$\begin{aligned} (\sigma + im\hat{\Omega}(x)) (\Delta_2 \Phi) + \left( \frac{\hat{\kappa}^2}{\hat{\Omega}} - 2\hat{\Omega} \right) (\Delta_2 V) \\ - \left( \frac{\hat{\kappa}^2}{\hat{\Omega}} - 4\hat{\Omega} \right) \frac{\partial}{\partial x} \left( \frac{\partial V}{\partial x} - \frac{im}{x} \Phi \right) \\ + 2f \left( \frac{d\hat{\Sigma}_0(x)}{dx} \frac{\partial \psi'}{\partial x} + \hat{\Sigma}_0(x) (\Delta_2 \psi') \right) \\ + \frac{1}{\mathcal{M}^2} \left( \Delta_2 (\hat{T} \Sigma') + \frac{1}{x} \frac{\partial}{\partial x} (n \hat{T} \Sigma') \right) = 0, \\ (\sigma + im\hat{\Omega}(x)) (\Delta_2 V) - \frac{\hat{\kappa}^2}{2\hat{\Omega}} (\Delta_2 \Phi) \\ - \left( \frac{d}{dx} \frac{\hat{\kappa}^2}{2\hat{\Omega}} \right) \left( \frac{\partial \Phi}{\partial x} + \frac{im}{x} V \right) \\ - 2f \frac{im}{x} \frac{d\hat{\Sigma}_0}{dx} \psi' + \frac{imn\hat{T}}{x^2 \mathcal{M}^2} \Sigma' = 0, \\ (\sigma + im\hat{\Omega}(x)) \Sigma' + \Delta_2 \Phi = 0. \end{aligned} \quad (17)$$

Here the characteristic scale,  $R$ , of the background density variation is used to measure distances,  $r = Rx$ , and  $\Sigma_0(R)$  is applied to normalize densities,  $\Sigma_0(x) = \Sigma_0(R) \hat{\Sigma}_0(x)$ .  $\Omega_0 = \Omega(R)$  may scale the angular velocity,  $\Omega = \Omega_0 \hat{\Omega}(x)$ ,  $\Omega_0^{-1}$  scales time,  $\Omega_0 R$  - the velocity, and  $2\pi G \Sigma_0(R) R$  - the gravity potential.  $\hat{T}(x)$  is the normalized temperature profile defined by the equation,  $c_{\text{ac}}^2 = C_{\text{ac}}^2 \hat{T}$ , where  $C_{\text{ac}}^2$  is the (constant) sound velocity at  $r = R$ , so that  $\hat{T}(1) = 1$ . We also keep in Eqs. (17) the same notations for the normalized flow potentials and normalized density and gravity disturbances as used before for the dimensional variables. Two governing parameters of Eqs. (17),

$$\mathcal{M} = \frac{R\Omega_0}{C_{\text{ac}}}, \quad f = \frac{\pi \Sigma_0 G}{R\Omega_0^2}, \quad (18)$$

are the Mach number and the  $f$ -parameter, which for Keplerian disks with  $\Omega_0^2 = GM_*/R^3$  becomes the fractional disk mass,  $f = \pi R^2 \Sigma_0 / M_*$ .  $\mathcal{M}$  and  $f$  can be combined into the global Toomre parameter (2),

$$Q = 1/(f\mathcal{M}). \quad (19)$$

### 3. Spectral formulation

There are at least two clear advantages for a change to the spectral formulation by applying the Fourier-Bessel transforms. First, it yields simple solution (10) of the Poisson equation (9) for the gravity potential. Second, the typical singularities of the problem like that of the Keplerian

angular velocity,  $\Omega \sim x^{-1.5}$ , at the origin,  $x = 0$ , are easily integrable with the Bessel functions. Hence, we do not need to introduce any internal boundary. The physical internal boundary presented by the surface of the central star is not important because its radius is normally several orders of magnitude smaller than the radius of the disk.

We drop the time and azimuth dependencies in the Fourier–Bessel expansions to write

$$\begin{aligned}\Delta_2 \Phi(x) &= \int_0^\infty J_m(kx) k \tilde{\Phi}(k) dk, \\ \Delta_2 V(x) &= \int_0^\infty J_m(kx) k \tilde{V}(k) dk, \\ \Sigma'(x) &= \int_0^\infty J_m(kx) k S(k) dk, \\ \psi'(x) &= - \int_0^\infty J_m(kx) S(k) dk,\end{aligned}\quad (20)$$

where the last equation gives the (normalized) solution of the Poisson equation (9) in the disk plane. Note that  $\tilde{\Phi}$  is the spectrum for  $\Delta_2 \Phi$ , while the spectrum for  $\Phi$  is  $-k^{-2} \tilde{\Phi}$ , and the same about  $V$ .

The expansions (20) lead to the spectral formulation of the eigenvalue problem, i.e.

$$\begin{aligned}\sigma \tilde{\Phi}(k) &= -im \int_0^\infty R(k, k') \tilde{\Phi}(k') dk' \\ &\quad - 2 \int_0^\infty R_1(k, k') \tilde{V}(k') dk' \\ &\quad + 2f \int_0^\infty D(k, k') S(k') dk' \\ &\quad + \frac{1}{\mathcal{M}^2} \int_0^\infty T(k, k') S(k') dk', \\ \sigma \tilde{V}(k) &= -im \int_0^\infty R_2(k, k') \tilde{V}(k') dk' \\ &\quad + \int_0^\infty R_3(k, k') \tilde{\Phi}(k') dk' \\ &\quad + i2mf \int_0^\infty D_1(k, k') S(k') dk' \\ &\quad + \frac{im}{\mathcal{M}^2} \int_0^\infty T_1(k, k') S(k') dk', \\ \sigma S(k) &= -im \int_0^\infty R_4(k, k') S(k') dk' - \tilde{\Phi}(k),\end{aligned}\quad (21)$$

where the rotational ( $R, R_1, \dots, R_4$ ), density ( $D, D_1$ ), and temperature ( $T, T_1$ ) kernels are given in the Appendix.

All the kernels in Eqs. (21) are real functions. This simple observation leads to an important consequence. It follows that if  $S(k), \tilde{\Phi}, \tilde{V}$  is a solution with the eigenvalue  $\sigma = \gamma + im\Omega_p$ , then  $S^*, -\tilde{\Phi}^*, \tilde{V}^*$  is also a solution with the eigenvalue  $-\sigma^* = -\gamma + im\Omega_p$  (the upper script ‘\*’ means complex conjugate). To put it in other words, for each trailing (leading) global spiral pattern with

growth (decay) rate,  $\gamma$ , and the pattern speed,  $\Omega_p$ , there exists a correspondent leading (trailing) pattern with exactly the same pattern speed and decay (growth) rate  $-\gamma$ . This statement known as the anti–spiral theorem for the tightly–wound spiral waves (Lynden-Bell & Ostriker 1967) applies also to the global disturbances. The theorem is fully symmetric about leading and trailing patterns. The computations discussed in the Sect. 5.2 show, however, a remarkable difference between the two types of excitations. Only trailing structures may be unstable. The leading excitations either decay or have zero growth rates.

It may be also shown that when the typical scale of excitations,  $\ell \sim k^{-1}$ , is small compared to the scale of variations of the undisturbed disk parameters, so that the angular velocity, surface density and temperature may be considered uniform, the integral equation system (21) reduces to an algebraic equations reproducing well–known dispersion relation of the Lin’s theory for tightly–wound spiral density waves.

If the profiles of the angular velocity, the background density, and temperature are known, the kernels of the integral equations (21) can be explicitly defined and the (numerical) solution of the eigenvalue problem may be found.

### 3.1. Axisymmetry

Drastic simplifications can be found for azimuthally uniform disturbances indicating that some physics essential for the nonaxisymmetric (spiral) excitations is missing in the case of the axisymmetric (ring) disturbances.

For  $m = 0$ , the first two equations of the system (21) become

$$\begin{aligned}\sigma \tilde{\Phi}(k) &= -2 \int_0^\infty R_1(k, k') \tilde{V}(k') dk' \\ &\quad + 2f \int_0^\infty D(k, k') S(k') dk' \\ &\quad + \frac{1}{\mathcal{M}^2} \int_0^\infty T(k, k') S(k') dk', \\ \sigma \tilde{V}(k) &= \int_0^\infty R_3(k, k') \tilde{\Phi}(k') dk'.\end{aligned}\quad (22)$$

The remainder equation relates the divergence and density spectra

$$\sigma S(k) = -\tilde{\Phi}(k).\quad (23)$$

Substitution of this equation into (22)<sub>2</sub> gives the integral relation between vorticity and density spectra which does not include the eigenvalue:

$$\tilde{V}(k) = - \int_0^\infty R_3(k, k') S(k') dk'.\quad (24)$$

Next we substitute these two latter equations into (22)<sub>1</sub> to find the closed equation for the density spectrum,

$$\begin{aligned} \sigma^2 S(k) &= -k \int_0^\infty \mathcal{R}(k, k') S(k') dk' \\ &+ 2f \int_0^\infty \mathcal{D}(k, k') S(k') dk' \\ &- \frac{1}{\mathcal{M}^2} \int_0^\infty \mathcal{T}(k, k') S(k') dk'. \end{aligned} \quad (25)$$

The kernel functions for the axisymmetric case read

$$\begin{aligned} \mathcal{R}(k, k') &= \int_0^\infty \hat{\kappa}^2(x) x J_1(kx) J_1(k'x) dx, \\ \mathcal{D}(k, k') &= kk' \int_0^\infty \hat{\Sigma}_0(x) x J_1(kx) J_1(k'x) dx, \\ \mathcal{T}(k, k') &= kk' \int_0^\infty \hat{T}(x) (kx J_0(kx) \\ &- n(x) J_1(kx)) J_0(k'x) dx. \end{aligned} \quad (26)$$

For the case of Keplerian rotation,  $\hat{\kappa} = x^{-1.5}$ , we find

$$\mathcal{R}(k, k') = \frac{kk'}{2(k+k')} F\left(\frac{1}{2}, \frac{3}{2}; 3; \frac{4kk'}{(k+k')^2}\right), \quad (27)$$

where  $F$  is the hyper-geometric function. This expression holds with a neglect of the influence of self-gravity and pressure on the rotation law. The same approximation applied to an isothermal disk implies

$$\mathcal{T}(k, k') = k^2 \delta(k - k'). \quad (28)$$

All the kernel functions of Eq. (25) are symmetric in this approximation. The symmetry means that  $\sigma^2$  is real so that overstability is not possible. Only stable oscillations (negative  $\sigma^2$ ) and steadily growing or decaying eigenmodes (positive  $\sigma^2$ ) may be found.

#### 4. The model

The rotation law of the disk is defined by the radial equilibrium condition

$$r\Omega^2(r) = \frac{GM_\star}{r^2} + \frac{d\psi}{dr} + \frac{c_{ac}^2}{\Sigma_0} \frac{d\Sigma_0}{dr} \quad (29)$$

(Adams et al. 1989). The rotation law by Eq. (29) depends on the basic parameters (18) of the problem. This involves similar dependence in rotational kernels of the governing integral equations (21). Massive computations are, however, required to define the marginal stability parameters – one of the tasks by this study. For the sake of simplicity, we neglect in (29) the self-gravity and pressure contributions to deal with the Keplerian rotation case.

The surface density distribution is parameterized as follows,

$$\hat{\Sigma}_0 = \frac{x^{-p}}{(1+x^{lq})^{-1/l}}. \quad (30)$$

This profile describes the power law,  $\hat{\Sigma} \simeq x^{-p}$ , for  $x < 1$ , which changes to  $\hat{\Sigma} \simeq x^{-(p+q)}$  for  $x > 1$ . Parameter  $l$  defines how sharp is the transition between the two power laws. We adopt the values of  $l = q = 10$  to make the transition relatively sharp. With this choice, the surface density decreases rapidly with radius beyond the circle  $x = 1$ . Hence,  $x = 1$  defines the outer edge of the disk in our model. We avoid, however, imposing the outer boundary explicitly and shall formally consider an infinite disk. On this way we sidestep imposing the outer boundary conditions which are rather problematic to formulate consistently.

For the power index,  $p$ , of the density profile inside the disk Weidenschilling & Cuzzi (1993) favor  $p \simeq 1.5$  after considering the distribution of planets in the solar system. Cassen & Moosman (1981) found that the values in the range 0.5 – 2 are possible for protostellar disks. We assume  $p = 1$  in the present model.

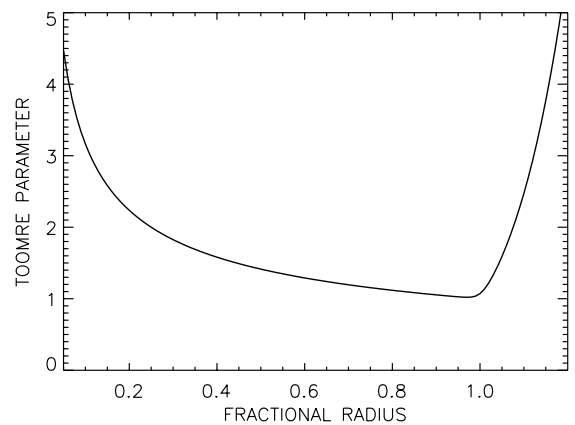


Fig. 1. Radial profile of the ‘local’ Toomre parameter

Temperature is assumed to be constant with position.

The disk stability is controlled by the Toomre  $Q$ -parameter, at least in the axisymmetric case. The global parameter value is defined by Eq. (19). The local values can be found by multiplying the global  $Q$  by the profile of Fig. 1. The figure shows that the region around the outer edge of the disk should be ‘most unstable’.

Assumptions of Keplerian rotation and thin-disk approximation imply that the fractional mass (18) is small and Mach number is large. We shall, however, consider fractional masses up to  $f = 1$  with hope that the model remains qualitatively valid even for not too small  $f$ .

This paper considers global (large-scale) excitations. We neglect short-wave contributions in the integral equations (21), (25) by replacing infinity in the upper limits of the integrals by some large but finite value  $k_0$ . Typically,  $k_0 \sim 50 - 100$  for the axisymmetric modes and  $k_0 \sim 100 - 200$  for nonaxisymmetric excitations provide

satisfactory accuracy. The integral equations were solved by Nystrom method using the Gauss–Legendre quadrature rule.

## 5. Results and discussion

Figure 2 shows the the stability diagram of the present model. A disk is stable if the Mach number is sufficiently low, i.e. temperature is sufficiently high. Assuming that some cooling mechanism is active, the point representing position of the disk on the parametric plane rises up with time. Eventually it invades the instability region. It seems plausible to expect that the type of the excitation produced by the instability is defined by the first marginal stability line crossed by the system trajectory. In this sense,

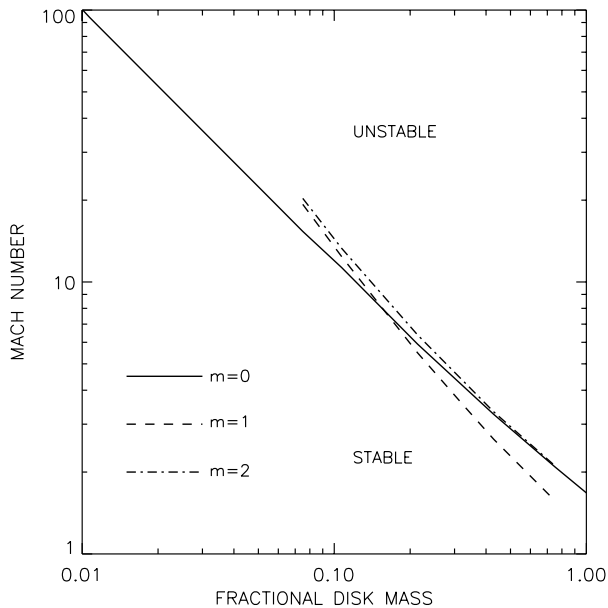


**Fig. 2.** Marginal stability lines for rings ( $m = 0$ ) and low- $m$  spirals

we expect the axial symmetry of the unstable disturbances to depend on the fractional mass. Relatively heavy disks ‘prefer’ one-armed spirals ( $m = 1$ ) while rings ( $m = 0$ ) are excited in tiny disks. The change of axial symmetry occurs at  $f \simeq 0.16$ .

### 5.1. Rings

The stability criterion,  $Q > 1$ , is reproduced closely only for very small fractional masses. Critical value of the global Toomre parameter (19) decreases slowly with  $f$  to become  $Q = 0.60$  for  $f = 1$ . The decrease is most probably related to the increase of spatial scale of the marginally stable excitations with fractional mass clearly seen in Fig. 3.

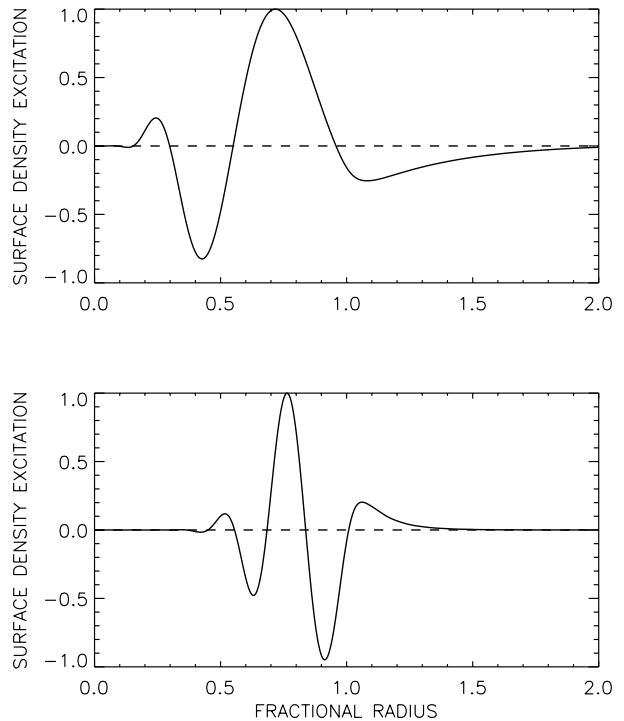


**Fig. 3.** Marginally stable axisymmetric density excitations for  $f = 0.5$  (top) and  $f = 0.1$  (bottom). Spatial scale of the eigenmodes increases with fractional mass

Figure 1 shows that when the global parameter (19) equals one, the local Toomre parameter does so only in one point close to the edge of the disk where the parameter attains its minimum value. Only the excitations strongly concentrated to this point may be unstable with  $Q$  slightly below one and only the small-scale eigenmodes for very low  $f$  can satisfy the condition. When fractional mass is not too small, the scale of the marginally stable excitations become comparable to the size of the disc. The excitations cover a range of axial distances where local Toomre parameter exceeds considerably its minimum value. Hence, the large-scale excitation require the global  $Q$ -parameter to sink considerably below one to become unstable.

Figure 3 shows also that one or two density maxima are dominating the density excitation profiles (note that the linear analysis can not define the sign of the eigenmodes so that the profiles with inverse sign also represent the marginally stable excitations). When a disk becomes unstable, rings are produced at its outer edge. The remainder of the disk has a smaller fractional mass. Hence, it requires further cooling for the instability to produce further rings.

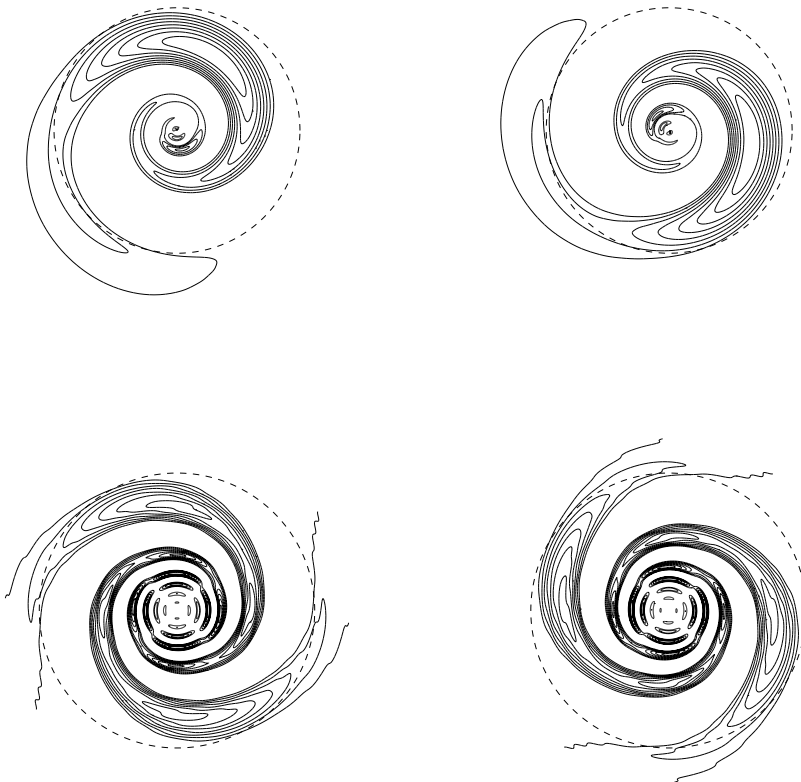


**Fig. 4.** Decaying (left) and growing (right) one-armed (top) and two-armed (bottom) spiraling excitations for  $f = 0.3$ . Only positive levels of density disturbances are shown. Broken circle indicates the disk edge,  $x = 1$ . The background rotation is anti-clockwise

## 5.2. Spirals

Two types of the nonaxisymmetric excitations can be identified with the present model. One of them we shall call spirals because of the shape of their surface density disturbances.

As fair as we can judge, the spectrum of spirals is discrete. The matrix equation representing the true integral equations in the numerical code, of course, always has a discrete spectrum. However, if we increase resolution by increasing the number of grid-points for a given range of wave numbers, the number of spiral-type excitations remains roughly constant indicating a truly discrete spectrum.

In accordance with the anti-spiral theorem (cf. Sect. 3), the spirals are always found in pairs with opposite sense of spiraling but identical pattern speeds. The problem, however, is that finite numerical resolution produces small but finite false real parts of the eigenvalues,  $\gamma \sim 0.01 - 0.1$ . By this reason, even for low Mach numbers where the system is definitely stable, the numerically-defined eigenvalues of the spiral and correspondent anti-spiral are not identical but possess small real parts with opposite signs. As the Mach number is increased, the pairs of eigenvalues are wandering along the imaginary axis,

$\Re(\sigma) = 0$ , until two pairs meet each other. After that, one pair remains on the imaginary axis while two other eigenvalues start moving perpendicular to this axis in opposite directions. Their real parts increase rapidly. We identify the bifurcation with the onset of instability.

No one example for growth of a leading spiral was found. They have zero growth rate or decay when the correspondent (trailing) anti-spiral becomes unstable. The examples of growing modes for the zonal wave numbers  $m = 1, 2$  are shown in the right panels of Fig. 4.

The gravitational instability represents a possible mechanism for planet formation. Though the alternative concept of planetesimals coagulation seems to be now days a leading one, the instability can not be finally rejected. The one-armed spirals is the most promising mode in this context. On the right-top part of Fig. 4 we see that the unstable mode has several density maxima which could be identified with future planets. The number of maxima depends on the fractional mass. Figure 5 illustrates the tendency: the number of the density concentrations decreases with  $f$ . Therefore, the heavy disks may be expected to produce binary companions or giant planets while multiple smaller planets may form in more light disks.

We did not try to reproduce the Titus-Bode law with this simple model. It may be noted, however, that Figs. 4

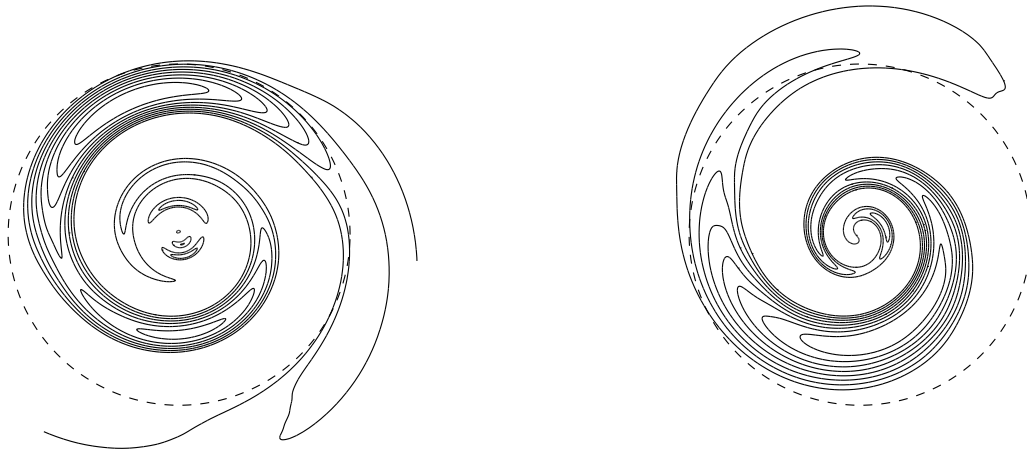


**Fig. 5.** Growing one-armed modes for  $f = 0.2$  (left) and  $f = 0.4$  (right). More surface density concentrations are produced with smaller fractional mass

and 5 display the correct tendency. The radial separation of subsequent density maxima increases with axial distance. The problem on how the excess of gas is removed from the protoplanetary condensations leaving heavy elements to form the planets remains, however, open after this model.

The preference of the one-armed nonaxisymmetric disturbances is, probably, a special feature of the disks around the massive central bodies. If the central mass were absent or small, the conservation of the center-of-mass position would preclude the  $m = 1$  instability in favor of the two-armed modes. In our case the central mass plies the role of the second arm. Also indirect potential neglected in our model reinforces the instability of the  $m = 1$  modes (Adams et al. 1989). An account for this effect would, most probably, shift the transition from rings to spirals in Fig. 2 to a smaller fractional mass.

### 5.3. Vortices

A typical example of the other type of nonaxisymmetric excitations is shown in Fig. 6. We call them ‘vortices’ because of close correlation between density and vorticity disturbances. In contrast to spirals, the eigenvalues of vortices are not degenerated and their real parts are strictly zero within the numerical precision. If resolution of the numerical model is increased, say, two times, the number of vortex-type eigenvalues is also roughly doubled indicating continuous spectrum.

On the right panel of Fig. 6 the stream-lines of the vortical flow, i.e. isolines of the vorticity potential,  $V$ , by Eqs. (12) and (13), are shown. The circulation around

the density maxima has the same vorticity sign as the background rotation and v.v. around the density minima. These circulation directions are opposite to that required for the geostrophic balance (Adams & Watkins 1995). Hence, what we find are not geostrophic vortices. Accordingly, the divergence of the flow excitation is not small but has the same order of magnitude as vorticity. As can be seen from the middle panel of Fig. 6, the divergence around some position in the disk changes sign when the position is passed by a density extremum. The change is from negative to positive for a transit of density maximum and from positive to negative for a minimum.

The vortices were never found to be unstable. They require some unspecified external driving for being excited.

There are several lines along which the present model can be improved. E.g., it may be noted that the stability diagram of Fig. 2 has the most consequential features on its low-right corner. Hence, an account for deviations from Keplerian rotation and finite disk thickness may be desirable.

*Acknowledgements.* This work was supported by the Deutsche Forschungsgemeinschaft and by the Russian Foundation for Basic Research (Project 96-02-00010G).

## A. Appendix: the kernel functions

The rotational kernel-functions of the integral equation system (21) read

$$R(k, k') = \int_0^\infty \hat{\Omega}(x) \left[ 2kx J_{m+1}(kx) J_{m+1}(k'x) \right]$$

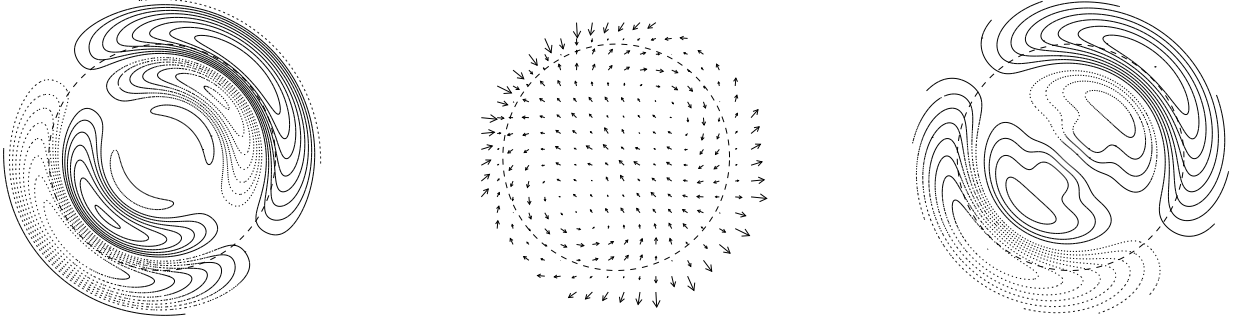


**Fig. 6.** An example of  $m = 1$  vortical excitation. From left to right: isolines of density disturbance, vector-plot of the mass flux,  $\Sigma_0 \mathbf{v}'$ , and stream-lines of the vortical flow. Full lines show positive density disturbances and anti-clockwise circulation. The global rotation is anti-clockwise. The disk parameters are:  $f = 0.2$ ,  $\mathcal{M} = 5$ . The pattern migrates in the direction of background rotation with the (normalized) speed  $\Omega_p = 1.99$

$$- \frac{2(m-1)}{k'} (kJ_{m+1}(kx)J_m(k'x) + k'J_m(kx)J_{m+1}(k'x)) + \left( \frac{4m(m-1)}{k'x} - k'x \right) J_m(kx)J_m(k'x) \Big] dx, \quad (\text{A1})$$

$$R_1(k, k') = \int_0^\infty \hat{\Omega}(x) \left[ kxJ_{m+1}(kx)J_{m+1}(k'x) + \frac{m(m-1)}{k'} (kJ_{m+1}(kx)J_m(k'x) + k'J_m(kx)J_{m+1}(k'x)) - 2\frac{m^2(m-1)}{k'x} J_m(kx)J_m(k'x) \right] dx, \quad (\text{A2})$$

$$R_2(k, k') = \int_0^\infty \hat{\Omega}(x) \left[ 2kxJ_{m+1}(kx)J_{m+1}(k'x) - \frac{2(m-1)}{k'} (kJ_{m+1}(kx)J_m(k'x) + k'J_m(kx)J_{m+1}(k'x)) + \left( \frac{4m(m-1)}{k'x} - kx\frac{k}{k'} \right) J_m(kx)J_m(k'x) \right] dx, \quad (\text{A3})$$

$$R_3(k, k') = \int_0^\infty \left\{ m\hat{\Omega}(x) \left[ -2kxJ_{m+1}(kx)J_{m+1}(k'x) + \frac{2(m-1)}{k'} (kJ_{m+1}(kx)J_m(k'x) + k'J_m(kx)J_{m+1}(k'x)) - \left( \frac{4m(m-1)}{k'x} - x\frac{(k^2 + k'^2)}{k'} \right) J_m(kx)J_m(k'x) \right] + kx\frac{\hat{k}^2}{2\hat{\Omega}} J_{m+1}(kx)J_{m+1}(k'x) \right\} dx, \quad (\text{A4})$$

$$R_4(k, k') = \int_0^\infty \hat{\Omega}(x) k'xJ_m(kx)J_m(k'x) dx. \quad (\text{A5})$$

For the Keplerian rotation law, these kernels can be expressed in terms of the hyper-geometrical functions similar to Eq. (27). Reliable numerical routines exist to compute the functions.

A closer examination of the relatively complicated expressions for the rotational kernels shows that all of them are linear combinations of more simple common blocks. The same is true about the density and temperature kernels:

$$D(k, k') = \int_0^\infty \hat{\Sigma}_0(x) \left[ -xkk'J_{m+1}(kx)J_{m+1}(k'x) + mkJ_{m+1}(kx)J_m(k'x) + mk'J_m(kx)J_{m+1}(k'x) - \frac{2m^2}{x} J_m(kx)J_m(k'x) \right] dx, \quad (\text{A6})$$

$$D_1(k, k') = \int_0^\infty \hat{\Sigma}_0(x) \left[ \frac{2m}{x} J_m(kx)J_m(k'x) - kJ_{m+1}(kx)J_m(k'x) - k'J_m(kx)J_{m+1}(k'x) \right] dx, \quad (\text{A7})$$

$$T(k, k') = kk' \int_0^\infty \hat{T}(x) \left[ \left( kx + \frac{mn(x)}{kx} \right) J_m(kx)J_m(k'x) - n(x)J_{m+1}(kx)J_m(k'x) \right] dx, \quad (\text{A8})$$

$$T_1(k, k') = -k' \int_0^\infty \hat{T}(x) \frac{n(x)}{x} J_m(kx)J_m(k'x) dx. \quad (\text{A9})$$

## References

- Adams F.C., Watkins R., 1995, ApJ 451, 314
- Adams F.C., Ruden S.P., Shu F.H., 1989, ApJ 347, 959
- Aoki S., Iye M., 1978, PASJ 30, 519
- Aoki S., Noguchi M., Iye M., 1979, PASJ 31, 737
- Beckwith S.V.W., 1994, Protoplanetary disks. In: Duschl W.J. et al. (eds.), Theory of accretion disks - 2. Kluwer, Dordrecht, p. 1
- Bertin G., 1983, A&A 127, 145

- Bertin G., Mark J., 1979, *SIAM J. Appl. Math.* 36, 407
- Binney J., Tremaine S., 1987, *Galactic Dynamics*. Princeton University Press, Princeton
- Cameron A.G.W., 1978, *Moon and Planets* 18, 5
- Cassen P.M., Moosman A., 1981, *Icarus* 48, 353
- Cassen P.M., Smith B.F., Miller R.H., Reynolds R.H., 1981, *Icarus* 48, 377
- Fuchs B., 1996, *MNRAS* 278, 985
- Goldreich P., Ward W.R., 1973, *ApJ* 183, 1051
- Haass J., 1983, In: *Proc. of the Workshop on the Milky Way, Kinematics, dynamics and structure of the Milky Way*. D. Reidel Publishing Co., Dordrecht, p. 283
- Hayashi C., Nakazawa K., Nakagawa Y., 1985, In: Black D.C., Matthews M.S. (eds.) *Protostars & Planets II*. Univ. Arizona Press, Tucson & London, p. 1100
- Hohl F., 1971, *ApJ* 168, 343
- Köhler R., 1995, *A&A* 294, 690
- Lin C.C., Shu F.H., 1964, *ApJ* 140, 646
- Lissauer J.J., Cuzzi J.N., 1985, In: Black D.C., Matthews M.S. (eds.) *Protostars & Planets II*. Univ. Arizona Press, Tucson & London, p. 920
- Lynden-Bell D., Ostriker J.P., 1967, *MNRAS* 136, 293
- Meinel R., 1983, *Astron. Nachr.* 304, 65
- Möhlmann D., 1985, *Moon and Planets* 33, 201
- Monaghan J.J., Lattanzio J.C., 1991, *ApJ* 375, 177
- Morfill G., Spruit H., Levy E.H., 1993, In: Levy E.H., Lunine J.I. (eds.) *Protostars and Planets III*. Univ. Arizona Press, Tucson & London, p. 939
- Nakagawa Y., Nakazawa K., Hayashi C., 1981, *Icarus* 45, 517
- Nieto M.M., 1972, *The Titius-Bode Law of Planetary Distances: Its History and Theory*, Pergamon Press, New York, London
- Polyachenko W.L., Fridman A.M., 1972, *AZh* 49, 157
- Rüdiger G., Tschäpe R., 1987, *Astron. Nachr.* 308, 349
- Safronov V.S., 1969, *Evolution of the Protoplanetary Cloud and the Formation of Planets (Israel Program for Scientific Translation)*
- Safronov V.S., Ruzmaikina T.V., 1985, In: Black D.C., Matthews M.S. (eds.) *Protostars and Planets II*. Univ. Arizona Press, Tucson & London, p. 959
- Schmit U., Tscharnuter W.M., 1995, *Icarus* 115, 304
- Shu F.H., 1985, In: Greenberg R., Brahic A. (eds.) *Planetary Rings*. p. 531
- Toomre A., 1964, *ApJ* 139, 1217
- Vauterin P., Dejonghe H., 1995, *A&A* 303, 721
- Yang S., Durisen R.H., Cohl H.S., Imamura J.N., Toman J., 1991, *Icarus* 91, 14
- Weidenschilling S.J., 1977, *Ap&SS* 51, 153
- Weidenschilling S.J., Cuzzi J.N., 1993, In: Levy E.H., Lunine J.I. (eds.) *Protostars and Planets III*. Univ. Arizona Press, Tucson & London, p. 1031